UR1993_11

1/23

TASMANIA
DEVELOPMENT
AND RESOURCES

Mineral Resources Tasmania
REPORT 1993/11

Tectonothermal evolution of the northwest Zeehan Quadrangle and contact metamorphism of the Oonah Formation by the Heemskirk Granite

by B. D. Goscombe

Abstract

The first deformational event (D_1) recognised in the Precambrian Oonah Formation was the most pervasive and intense. D_1 involved intense bedding-parallel foliation development and rare isoclinal folds; both accompanied the peak of regional metamorphism. The grade of regional metamorphism varies from sub-greenschist facies to greenschist facies in the very northwest corner of the Zeehan Quadrangle. Greenschist facies assemblages include chlorite-muscovite-quartz-calcite-plagioclase and plagioclase-tremolite-quartz-epidote. These possibly formed at typical greenschist facies temperatures of 300–400°C, and phengite geobarometry suggests pressures of 5250–6450 bar. These highest grade rocks may be equivalents of the Arthur Lineament.

D_1 tectonites experienced four phases of tight to open, inclined to upright folding (D_2–D_5) prior to deposition of Ordovician–Devonian sediments. The Oonah Formation in the most northwest portion of the Zeehan Quadrangle experienced approximately 18–22 km of uplift and denudation at some stage during the period between D_1 and Ordovician sedimentation. This uplift is a major tectonic event and may be the result of isostatic rebound in response to crustal overthickening during D_2–D_5 folding and horizontal crustal shortening.

The Early Carboniferous (347–351 Ma) Heemskirk Granite intruded and contact metamorphosed the Oonah Formation. The thermal aureole is very narrow and contains a variety of metamorphic assemblages according to the bulk rock chemistry. Such assemblages include andalusite-cordierite-biotite-muscovite-anthophyllite and garnet-chlorite-tourmaline-hornblende-anthophyllite-biotite in pelitic lithologies; and biotite-muscovite-tremolite-tourmaline ± plagioclase ± chlorite in quartzite lithologies. The hydrothermal aureole, defined by the presence of black tourmaline deposited in fractures and partially replacing pelitic layers in the Oonah Formation, is in part wider than the thermal aureole. The hydrothermal aureole is partially controlled by the distribution of pre-existing fractures/faults in the Oonah Formation.

Minerals from selected samples were analysed for geothermobarometry and equilibrium thermodynamics work. These analyses indicate that the maximum temperatures of the thermal pulse experienced by the Oonah Formation were approximately 450–535°C. This is consistent with the assemblages developed. Such extremely low thermal aureole temperatures suggest that the Heemskirk Granite was a relatively cool granitic melt at the time of emplacement. None of the geobarometers applied are considered reliable, but the preferred pressure during emplacement was 3.5–4 kbar (12–14 km). This pressure estimate indicates a significant uplift and denudation event subsequent to granite emplacement and prior to deposition of the Late Carboniferous Zeehan Tillite. This uplift may have accompanied south over north high-angle thrusting and asymmetrical west-trending folding (D_6).

INTRODUCTION

This report is based on remapping of the northwest portion of the Zeehan Quadrangle in 1991 and 1992. Structural relationships were largely elucidated by detailed mapping of the coastal section north of the Heemskirk Granite. These structural relationships were confirmed and further elaborated by mapping of the Oonah Formation throughout the inland exposures, and from the Late Carboniferous Zeehan Tillite. The only Ordovician–Devonian sequences mapped were those in the Duck Creek Syncline. No Eocambrian or Cambrian sequences were mapped.

Four samples of contact metamorphosed Oonah Formation (1196, 2536, 1208A and 91-9) were collected and the constituent minerals analysed. Sample 2536 was collected by A. V. Brown at a confidential locality near Trial Harbour. All other samples were collected by B. D. Goscombe; the sample locations are shown in Figure 1. Samples prefixed by TH came from outcrop adjacent to the Heemskirk Granite at Trial Harbour. Only two of the four samples proved useful for geothermobarometry work. The temperature of contact metamorphism is useful in indicating a minimum temperature estimate for the granitic magma during Heemskirk Granite emplacement, whereas a pressure estimate at the time of emplacement is an important constraint on tectonic modelling of the region during the Early Carboniferous.

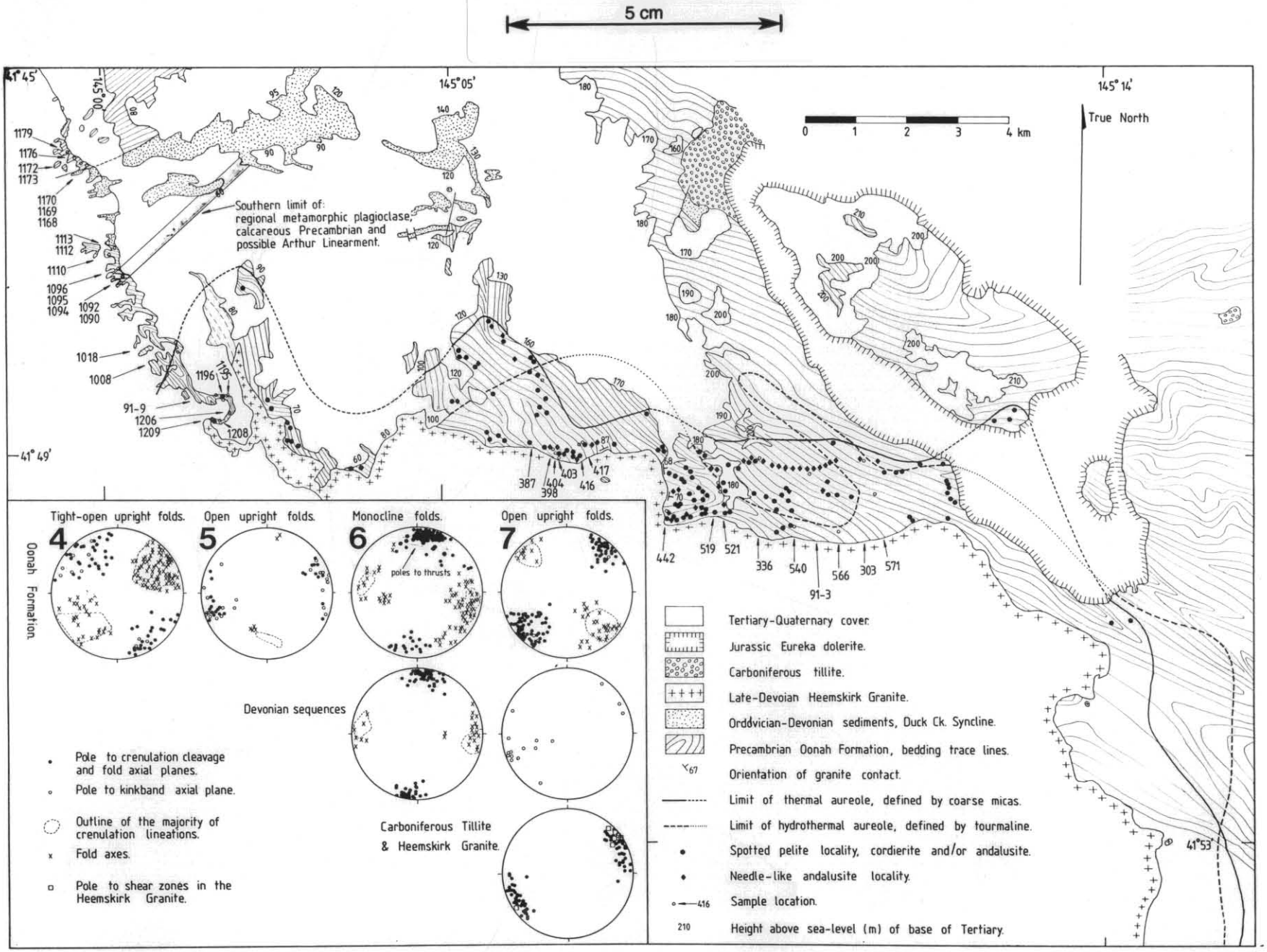

Figure 1. Simplified map of the northwest portion of the Zeehan Quadrangle. The locations of samples referred to in the text are shown and the thermal and hydrothermal aureole of the Heemskirk Granite outlined. Lower hemisphere equal area stereonets of D4 to D7 structural data, from different lithostratigraphic units, are contained in the inset.

2/23

TECTONOTHERMAL EVENTS

The tectonic and metamorphic episodes which are recognised in the area mapped are discussed here in chronological order. The whole sequence of tectonic events has been recognised in the well-exposed coastal section north of the Heemskirk Granite. This information was verified and further enhanced by analysis of inland exposures. A concise summary of the tectonic framework is contained in Table 1. For the following discussion D stands for a deformational event and all the structural expressions formed in that event (i.e. folds, thrusts, lineations foliations, shear planes etc.). These deformations have been labelled in chronological order based on overprinting criteria in the field. Each deformational event does not necessarily constitute a distinct orogenic period. Two or more of these deformations may have formed, in sequence, during the one orogeny.

Periods of postulated uplift and denudation (i.e. corresponding with unconformities) have been labelled separately because the tectonic nature of these events is not known, and they may all in fact be passive isostatic rebound events with no crustal shortening occurring at the time of uplift.

PRECAMBRIAN LITHOLOGIES

The oldest recognised rock unit in the Zeehan Quadrangle is the Oonah Formation. This formation constitutes the intensely and multiply-deformed schistose and layered quartzite-rich sequences. The dominant lithology is impure quartzite with thin (centimetre scale) bands of micaceous quartzite and quartz-rich pelitic laminations. Thicker (tens of metres scale) sequences of shale and siltstone are common. Less common lithologies are black graphitic and pyritic shales and rare volcanic and calcareous sequences.

The Precambrian rocks exposed in the coastal section north of the Heemskirk Granite are lithologically distinct, but are gradually transitional to those developed inland. Typical schistose quartz-rich lithologies of the inland Oonah Formation occur immediately north of the Heemskirk Granite. These calcareous schistose quartzites gradually increase in carbonate (calcite) content to the north. They are interlayered with minor muscovite-chlorite schist and shale, and rare units of mafic chlorite–tremolite-rich schist. The proportion of calcareous lithologies and mafic schists increases northward along the coastal section.

D_1 — ISOCLINAL FOLDS, INTENSE FABRICS AND METAMORPHISM

The earliest formed folds are recumbent isoclines with an intense fold axial planar penetrative foliation (S_1). D_1 folds are only rarely observed and have only been seen in the coastal section, although Brown (1986) has recognised two generations of isoclinal folding inland. D_1 folds are small scale (40–500 mm wavelength), isoclinal to very tight folds. They range widely in orientation, plunging 10–40° to the north, south and northwest (fig. 2); this was caused by later refolding. D_1 fold axes also vary widely in plunge within the one outcrop, although all of these axes are contained within the same fold axial plane. This geometry

Table 1.

Summary of the tectonothermal events recognised in the northwest portion of the Zeehan Quadrangle.

Ma	Age	Lithology	Metamorphism	Deformation	Structures
	to Present			Uplift #4	
	Tertiary	Gravel and sand			
				Uplift #3	
175–185	Middle Jurassic	Dolerite intrusion			
				D_{7b}	Open upright folds, 166°
				D_{7a}	Open upright folds, 145°
280–320	Late Carboniferous	Tillite deposition		?	
				Uplift #2	
347–351	Early Carboniferous	Heemskirk Granite	Contact metamorphism 450–535°C 3500–400 bar	?	
				D_6	S over N monoclines and thrusts, E–W.
500–380	Ordovician–Devonian	Sedimentation and burial.		Uplift #1	
				D_5	Open upright folds, N–S
				D_4	Open-tight upright folds, NE–SW.
				D_3	Tight inclined folds, NW–SE.
				D_2	Tight inclined folds, N–S.
	Precambrian	Quartzite-shale deposition and burial	Regional greenschist–sub-greenschist metamorphism ≤300–400°C 5250–6450 bar	D_1	Isoclinal folds and intense bedding parallel foliation (S_1).

suggests rotation of D_1 fold axes during D_1 deformation, not refolding by later fold events. Non-colinear folding such as this is typical of non-coaxial shear (Goscombe, 1991*b*).

S_1 foliation is defined by well-aligned phyllosilicates and elongate aggregates of quartz. S_1 is regionally pervasive, being developed in all outcrops of the Oonah Formation, and is nearly always subparallel to bedding. S_1 is the most intense penetrative planar foliation developed in the Oonah Formation, typically being slaty or schistose in nature, and in some quartz-rich localities has a sub-mylonitic appearance. C-S fabrics and asymmetrically-enclosed quartz vein augen have been recognised. All other planar fabrics associated with folding in the Oonah Formation are either crenulation cleavages (D_4 to D_7) or locally developed, spaced planar cleavages (D_2 and D_3). S_1 has a very wide range of orientation but in general dips towards the east (fig. 2). Thus D_1 may well have involved, very approximately, an east over west sense of transport. However, in the coastal section, C-S type S_1 fabrics indicate tectonic transport of southwest or west over towards the northeast or east.

Coeval with this foliation is a well-defined mineral elongation lineation were D_1 isoclines are prevalent. These are defined by elongate ribbons of fine-grained quartz aggregate. L_1 mineral elongation lineations are approximately parallel to the D_1 fold axes in the vicinity. Some competent beds are boudinaged and partially necked and attenuated by the S_1 fabric. The axis of extension associated with this boudinaging is parallel to the L_1 mineral elongation lineation. This boudinage axis of maximum extension ranges in orientation from plunging 20–44° towards 206° to 296°. Intersection lineations between bedding planes and S_1 plunge 0–45° towards the northeast to east.

The highest grade regional metamorphic minerals (chlorite, muscovite and tremolite) are developed within, and aligned to, the fold axial planar S_1 foliation. Consequently, the peak of regional metamorphism coincides with D_1 folding. Minerals in the S_1 foliation are crenulated, kinked and folded by all the subsequent deformational events (D_2–D_7), with no new mineral grains or new mineral phases developed within the fold axial planes of these later folds and crenulations. Thus all post-D_1 deformations occurred at lower temperatures of regional metamorphism than experienced during D_1.

In the coastal section the grade of peak regional metamorphism (M_1) in the Oonah Formation is variable between lower greenschist to greenschist facies, with the grade of metamorphism apparently increasing northward along the coastal section (fig. 3; Table 2*b*). Muscovite-chlorite-quartz assemblages occur throughout the whole sequence. Biotite never occurs in the regionally metamorphosed Oonah Formation; this mineral is indicative of the thermal overprint due to intrusion of the Heemskirk Granite, because the limit of biotite corresponds with the limit of coarse mica development used to define the limit of this aureole in the field. Progressing from south to north along the coastal section, the following progression in metamorphic assemblages are noted, ignoring the contact metamorphic overprint (fig. 3).

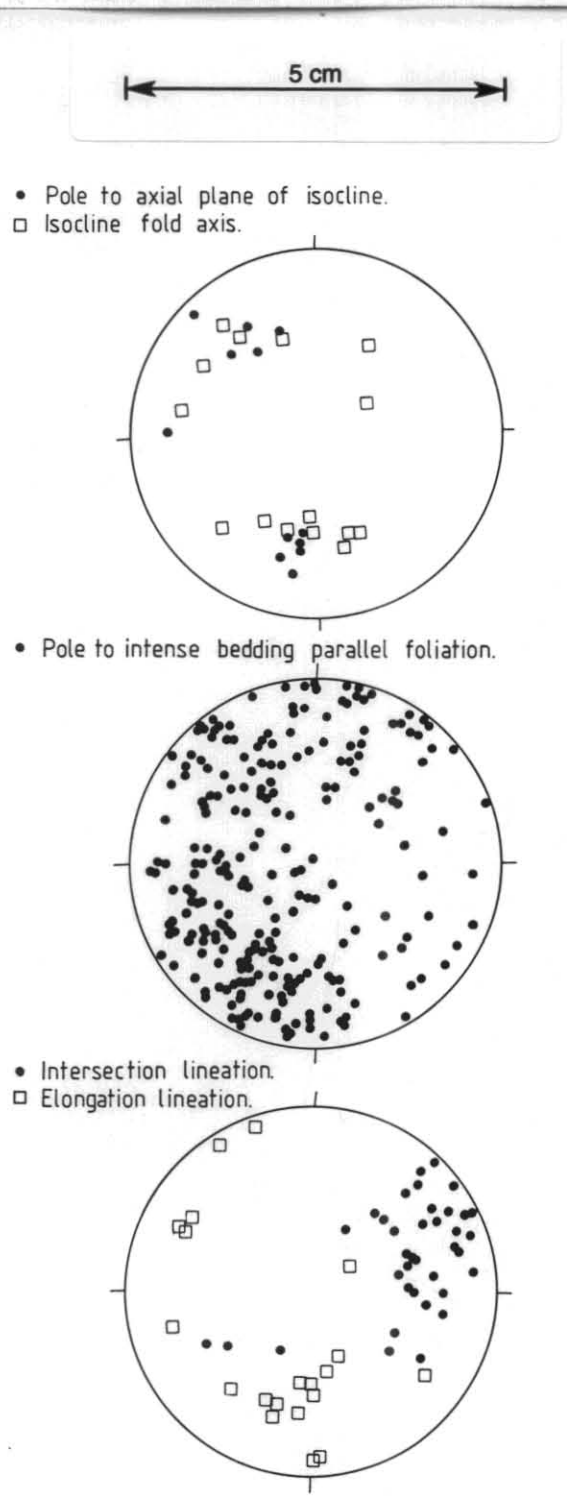

Figure 2.

Lower hemisphere equal area stereonets of D_1 structural data from the Oonah Formation.

(1) quartz-muscovite-chlorite

(2) quartz-muscovite-chlorite-calcite

(3) quartz-muscovite-chlorite-calcite-plagioclase

(4) quartz-muscovite?-chlorite-calcite-plagioclase-epidote-tremolite

These assemblages reflect a gradational change in metamorphic grade northward, as well as a gradational northward change in lithological types from quartz-rich lithologies to more calcareous compositions.

The grade of regional metamorphism of all the inland Oonah Formation outcrops is significantly lower than in

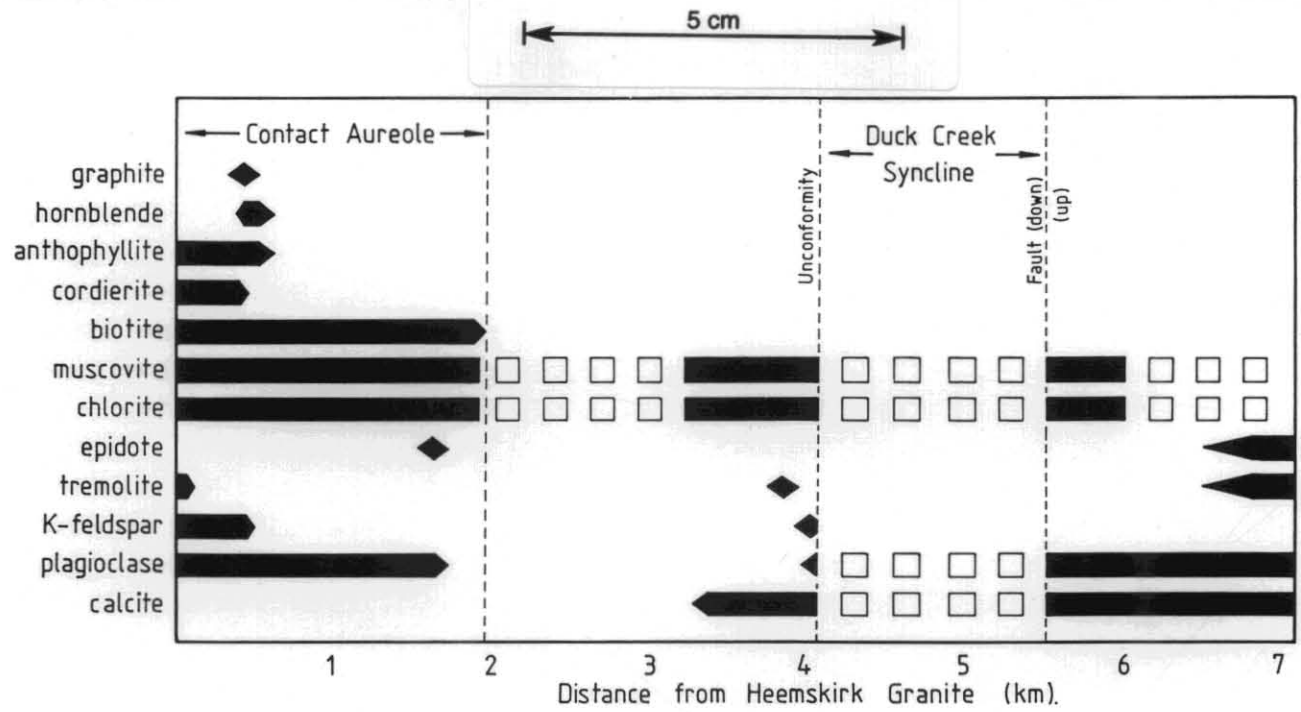

Figure 3.

Presence of mineral phases in the Oonah Formation of the coastal section, with respect to distance from the Heemskirk Granite towards the north.

the coastal section. Inland exposures are predominantly sub-greenschist (mostly lacking chlorite) shale and quartzite presumably containing illite, smectite, sericite, quartz, graphite and clay minerals. The tourmaline in these samples is detrital or hydrothermal in origin.

The higher metamorphic grades and occurrence of calcareous and mafic schist intercalations in the northern portion of the coastal section suggests that these rocks are part of the Arthur Lineament. The southern boundary of this zone is transitional, not only lithologically but also in metamorphic grade as discussed above. If a boundary was to be placed it would be at the first outcrops of calcareous quartzite (fig. 1). Na-plagioclase is first developed a further 600 m north of this 'boundary'; this is immediately below the unconformity on the southern margin of the Duck Creek Syncline. The presence of plagioclase south of the Duck Creek Syncline suggests that the increase in metamorphic grade to the north is potentially gradational and not entirely the result of the rocks in the north being upfaulted from deeper crustal levels and higher metamorphic grade (fig. 3). In addition to the change in metamorphic assemblages to the north, there is a progressive increase from south to north in the grainsize and degree of 'crystalline-metamorphic' nature of the rocks.

D_2 AND D_3 — TIGHT FOLDING DEFORMATIONS

Subsequent to D_1, the Oonah Formation experienced at least two generations of tight, inclined folding (D_2 and D_3). These tightly fold the pre-existing intense S_1 fabric. In the coastal section north of the Heemskirk Granite the fold axial planes trend 170–180° and 120–140° respectively for D_2 and D_3 (fig. 4). Fold axial planes are moderately to steeply inclined (dipping 30–90°) both to the east and west or NE and SW. Both these fold generations developed weak fold axial planar slaty cleavages, and no mineral elongation lineations were developed.

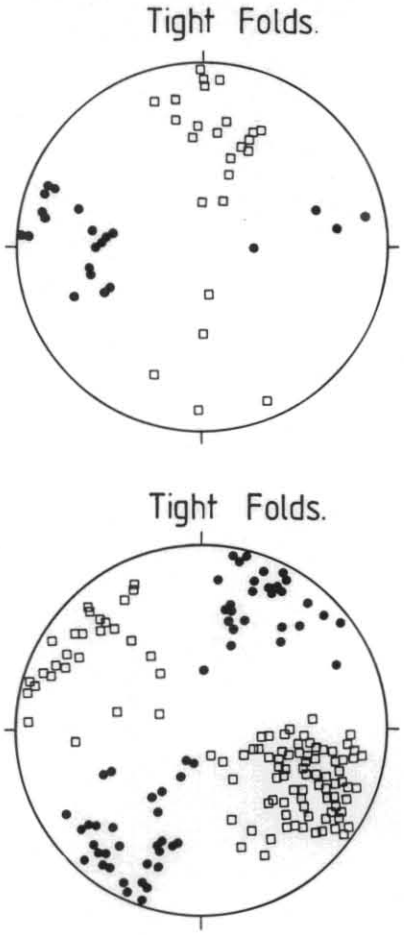

Figure 4.

Lower hemisphere equal area stereonets of D_2 (top) and D_3 (bottom) tight folding structural data from the Oonah Formation.

D_4 — TIGHT TO OPEN FOLDING DEFORMATION

D_4 folding is the dominant fold event in the Oonah Formation. Fold axis trends span a large range (30–80°) and plunge moderately to shallowly (0–60°) towards both the NE and SW (fig. 1). Fold axial planes dip moderately (90–50°) to both the NW and SE, although the majority of folds are essentially upright. The majority of crenulation cleavages and crenulation lineations associated with tight folds are of this generation. These NE-trending folds are found in outcrop and map scale, and are tight to open with interlimb angles ranging from 20–120°.

In shales, crenulation cleavages are developed fold axial planar to these folds. The width or wavelength of crenulations range from <1 mm to 10 mm and average 2.5 mm. These crenulations vary widely in their spacing, ranging from one to 80 mm with an average of 16 mm. Crenulation wave lengths wider than 10 mm have been arbitrarily called kink bands. Kink bands of, on average, 22 mm width are also developed fold axial planar to these folds. NE-trending crenulations and kink bands pre-date all other crenulations and kink bands. The following temporal sequence of D_4–D_7 fold events are constrained by overprinting crenulation criteria in Oonah Formation rocks. This sequence is further substantiated by the presence or absence of crenulation or kink band trends in younger rock sequences (i.e. Duck Creek Syncline and Zeehan Tillite), as discussed below.

D_5 — OPEN FOLDING DEFORMATION

Rare N-trending open-closed, upright folds are recognised in the Oonah Formation of the coastal section only. These folds have shallow plunges of <20° towards 010° and 190°. Fold axial planes are very steep, with dips >70° to both the east and west. North-trending kink bands are considered to be associated with this fold generation (fig. 1).

UPLIFT PERIOD #1

Subsequent to the D_1–D_5 folding events, the Oonah Formation was uplifted and denuded prior to deposition of the Ordovician–Devonian sedimentary sequences. The timing of this uplift (post-D_5, pre-D_6) with respect to the folding events is based on D_6 and D_7 being the only fold generations recognised in the Ordovician–Devonian Duck Creek Syncline. The absolute age of uplift and formation of the basal unconformity is not known. There may have been a multitude of uplift and denudation events subsequent to the Precambrian and during the Cambrian. Total uplift and denudation during this period may have been as great as 18–22 km, as indicated by one pressure estimate from regionally-metamorphosed Oonah Formation rocks (see mineral chemistry below).

A multitude of fault trends have been recognised during mapping (fig. 5). Most faults (excluding D_6 thrusts) are steep (90–60° dips) and range in trend from east-west to SE-NW. Most thrusts trend NW-SE and dip 70–50° to the northeast, and most normal faults trend east-west to ESE-WNW with steep northerly dips. A north-south set of near-vertical to westerly-inclined faults is recognised in the coastal section. Most faults are sharp discrete planes with

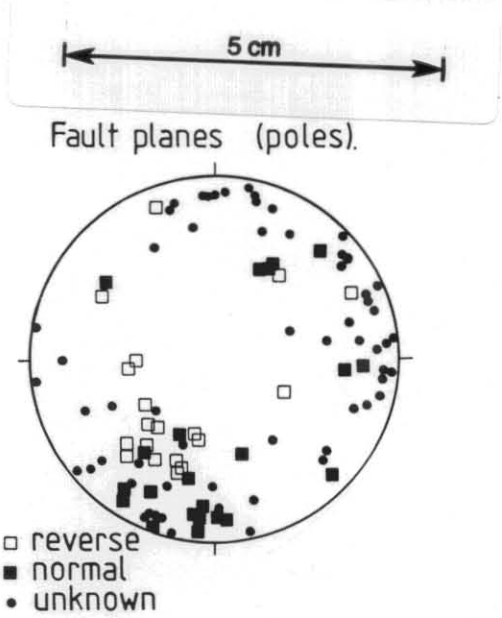

Figure 5.

Lower hemisphere equal area stereonet of reverse and normal fault plane orientation data from the Oonah Formation, excluding D_6 thrusts.

no brecciation. The few breccia zones recognised are typically <20 cm wide and contain carbonate in the breccia matrix. Displacements in all faults recognised in the coastal section are small, typically 100–400 mm, although some of >10 m displacement have been recognised.

No confident overprinting constraints are available to correlate any of the four uplift episodes, recognised in the region (Table 1), with a set of fault orientations. However, the following constraints are available.

(1) The common NW-SE fault trend (fig. 5) is inferred to have existed prior to intrusion of the Heemskirk Granite in the Early Carboniferous, as this pre-existing trend influenced hydrothermal fluid flow during intrusion (discussed below). This fault trend was, however, later reactivated because NW-trending faults are recognised in the Heemskirk Granite, and Tertiary deposits are displaced vertically by faults of this orientation (fig. 1).

(2) East-trending faults may have occurred after deposition of the Ordovician–Devonian sequences. This is based on the northern boundary of the Duck Creek Syncline being an east-trending faulted boundary. This fault may have had significant displacements because it is within a 1–5 m wide zone of brecciation and contorted rocks.

ORDOVICIAN – DEVONIAN SEDIMENTS OF THE DUCK CREEK SYNCLINE

A sequence of Ordovician–Devonian sediments was mapped in the coastal section at Duck Creek and immediately inland. The synformal structure in which the rocks are contained has been called the Duck Creek Syncline. In the coastal section the southern margin of these outcrops is an unconformity, and the northern margin is a 0.5 m wide fault within a broader breccia zone (fig. 6).

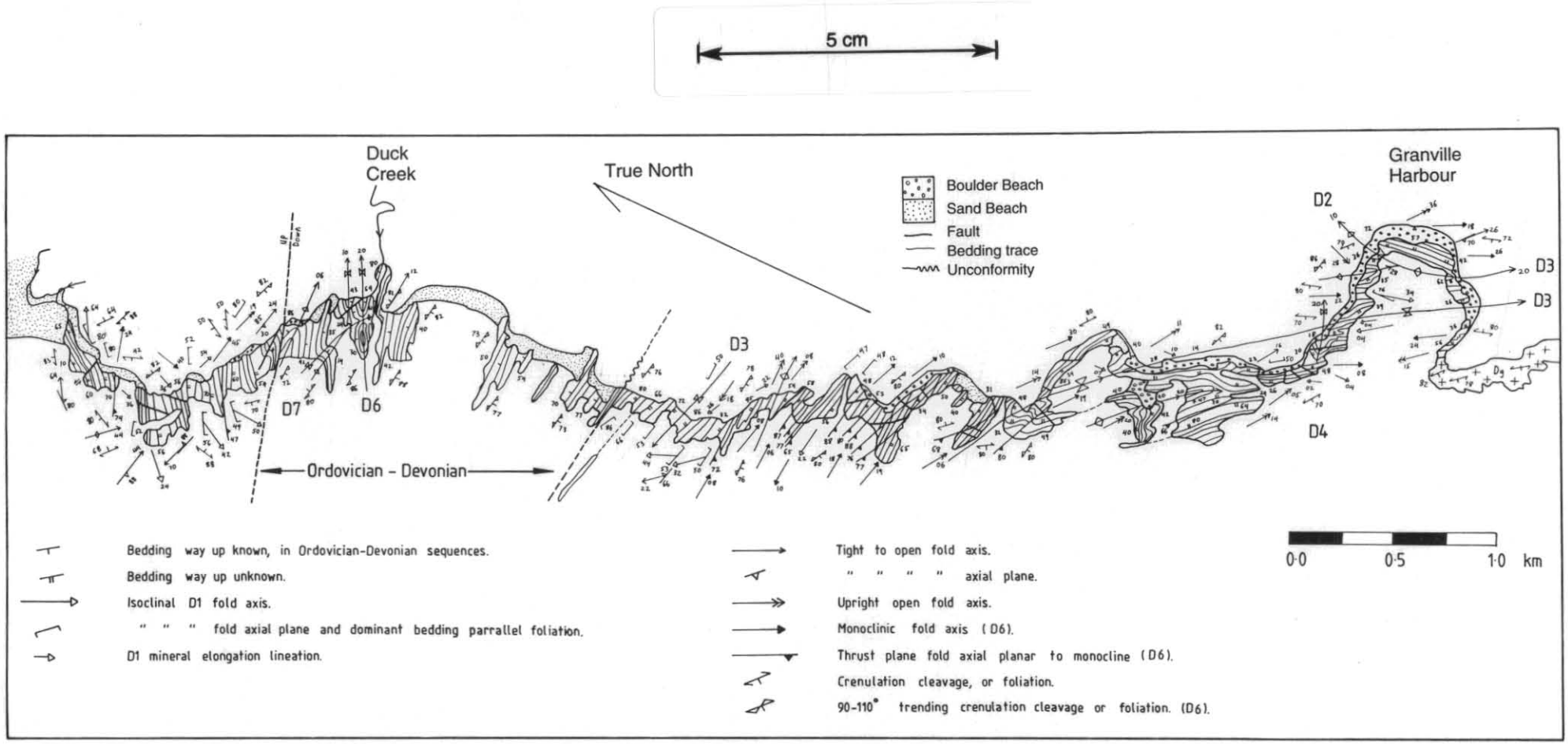

Figure 6. Detailed structural map of the coastal section north of the Heemskirk Granite.

7/23

The base of this sequence is a 12 m thick unit of clast-supported conglomerate, which grades up to conglomerate with a calcareous sandstone matrix and carbonates with pebbly bands. These gravelly carbonates grade into black-pink-grey-cream limestone of ≥33 m thick. This is overlain by a 61 m thick sequence of black calcareous shale, and then a 69 m unit of pale carbonate and calcareous sandstone. The bulk of the subsequent sequence comprises massive grey-green silty sandstone units without distinct bedding; these grade from calcareous to non-calcareous up sequence. The central portion of the synform consists of well-bedded sandstone beds with interbedded siltstone and silty sandstone; this unit is non-calcareous. The uppermost units consist of black calcareous shale and siltstone right up to the faulted boundary.

Inland sequences contain silicified quartz-rich conglomerate at the base. The rest of the sequence consists of silty sandstone with interbedded grey shale and siltstone.

D_6 — MONOCLINES AND THRUSTING DEFORMATION

Monoclines and associated high-angle thrusts have been observed in the coastal section. Steep (75–85° dips) south-dipping thrusts form discrete planes that are fold axial planar to asymmetrical monocline folds. The reverse sense of movement of the thrusts is consistent with the tectonic transport vector that formed the asymmetrical monocline folds. Displacements are typically very small, being mostly <200 mm. The middle limb of most monoclines has been attenuated and sheared by these thrust planes. Consequently, the thrusts are considered to have formed at a late stage during the same deformation episode as monocline development. Thrust and fold asymmetry is invariably due to SSW over NNE tectonic transport.

D_6 monoclines trend 90–110° and mostly plunge 0–20° to the ESE (fig. 1). Fold axial planes trend 90–110° and are predominantly inclined 70–90° to the south. The thrust planes have identical orientation to the fold axial planes of the monoclines (fig. 1). Monoclines are typically of only 300–500 mm amplitude. Interlimb angles are highly variable; most are true monoclines with interlimb angles of ≥90°, some are asymmetrical folds with interlimb angles of 30–90°. Monocline axes can be traced for tens of metres and thrusts can be traced for up to 800 metres. The thrusts represent the last stage of shortening when D_6 strain could not be accommodated volumetrically by ductile monoclinic folding.

East-trending open upright warp folds are also recognised in the Oonah Formation, these probably forming during D_6. The east-trending crenulation cleavage is very common throughout the whole area of Oonah Formation exposure. Kink bands of E-W trends, and on average 20 mm wide, are developed throughout the Oonah Formation.

Upright, open folding of 80–100° trend and 0–10° plunges to the east and west is recognised as the first deformation in the Ordovician–Devonian sequences of the Duck Creek Syncline. These folds are of 100–1000 m wavelength, and in fact the 2–3 km wide synformal nature of the Duck Creek Syncline itself is due to this open folding (fig. 6). A spaced planar cleavage with a trend of 90–110° and steep (80–90°) dips to both the north and south (fig. 1) is developed in these sediments. This cleavage is fold axial planar to the large-scale open folds. Because of the identical trend of these folds with the monoclines in the Oonah Formation the two are correlated. This correlation is further enhanced by the presence of a few similarly-oriented thrust planes, with south over north transport, within the Ordovician–Devonian sequence.

A conjugate set of sygmoidal quartz-filled tension gashes is recognised in the Ordovician–Devonian sequences. Dextral zones are steep and trend 150–158°, while sinistral zones are steep and trend 024–047°. This geometry suggests that an approximately N-S directed horizontal compressive stress formed these sygmoidal tension gash zones. This direction of maximum compressive stress is equivalent to that experienced during D_6 folding, and thus the gashes are correlated with D_6.

Monoclinic folds and associated thrusts are developed heterogeneously throughout the area mapped. Zones of high spatial concentration of thrusts and monoclines are identified in the continuous coastal section (fig. 6). Thus the strain associated with D_6 deformation was heterogeneously partitioned throughout the region. D_6 monoclines are small and the associated thrusts involved small displacements, thus bulk shortening for individual D_6 fold thrusts was not large. However, D_6 monoclines-thrusts, crenulation cleavages, kink bands and open folds are, as a group, the second most (after D_4) prevalent ductile structures other than D_1, and they are widely distributed. Thus D_6 deformation as a whole may have involved significant crustal shortening.

The timing of D_6 deformation is only loosely constrained in absolute time. As discussed, the Ordovician–Devonian sequences of the Duck Creek Syncline experienced D_6 deformation and the Late Carboniferous Zeehan Tillite did not. This constrains D_6 to between approximately 380 and 320 Ma (Table 1). No east-trending structures have been recognised in the Early Carboniferous Heemskirk Granite. D_6 strain may have been partitioned preferentially into the surrounding, less competent Oonah Formation. Thus the absence of D_6 structures in the granite body may not reflect a pre-granite D_6 deformation age. Consequently, the timing of D_6 cannot be more tightly constrained than the 380–320 Ma range.

EARLY CARBONIFEROUS HEEMSKIRK GRANITE INTRUSION AND CONTACT METAMORPHISM

The Heemskirk Granite is an extremely boron-rich granite that was emplaced into the Oonah Formation in the Early Carboniferous (347–351 Ma; Brooks and Compston, 1965). High boron contents are attested by the very high modal abundance of disseminated tourmaline and large (up to 150 mm diameter) spherical tourmaline-quartz nodules. This body also contains numerous late-stage laminated quartz-tourmaline dykes and veins; these typically trend SE–NW. These features indicate that a post-solidification boron/silica-rich fluid phase was present in the granite body. This late-stage fluid is considered to be the source of the voluminous tourmaline and quartz deposited within the Oonah Formation within the hydrothermal aureole of the Heemskirk Granite. Within the Oonah Formation,

tourmaline is crystallised in thin fractures and joints as well as centimetre-scale quartz-tourmaline veinlets. Tourmaline also crystallised within pelitic laminations in preference to quartz-rich layers in the Oonah Formation, resulting in a distinctive black and white stripped rock. This preferential precipitation of tourmaline in pelitic layers suggests that the hydrothermal fluids migrated through the body of the rock as well as along fractures and faults. The hydrothermal aureole, defined by the presence of tourmaline ± silica veinlets, is quite irregular (0–3 km) and has a 3 km long 'apophysis' trending to the northwest from the northern margin of the granite (fig. 1). This feature may be due to a pre-existing subsurface fault controlling fluid migration, or alternatively a subsurface extension of the Heemskirk Granite. Post-Tertiary faulting occurred along this zone, as indicated by the vertical displacement of Tertiary sediments (fig. 1). This post-Tertiary faulting may have reactivated an earlier fault zone.

The original source of the boron in the Heemskirk Granite was presumably the deeper crustal rocks that were partially melted during granite magma generation. The deeper crustal rocks may be Oonah Formation equivalents. This is supported by the common presence of accessory tourmaline in Oonah Formation shale and quartzite at a great distance from the Heemskirk Granite (at such distances that this tourmaline is not considered to be late-stage hydrothermal tourmaline).

The thermal aureole of contact-metamorphosed Oonah Formation is defined in the field by the presence of either euhedral andalusite crystals in the black shale, coarse white to pale green micas developed in pelitic laminations in the Oonah Formation, and less commonly by cordierite spots developed in the same. Mineralogically, the presence of biotite is diagnostic of the maximum limit of contact metamorphic effects, as it is not developed in any regionally-metamorphosed Oonah Formation lithologies. The thermal aureole is thin, with widths of 1–2 kilometres. Where exposed, the granite–Oonah contact is very steep, typically dipping 70–90° (fig. 1). Such steep contacts suggest that the middle levels of the pluton are presently exposed, the shallow-dipping upper surface of the pluton having already been eroded.

UPLIFT PERIOD #2

This second period of uplift, like the first uplift period, involved a significant amount of uplift and must be related to a major tectonic event. Granite clasts are recognised in the Late Carboniferous Zeehan Tillite (Goscombe, 1991*a*). These are thought to be sourced from the Early Carboniferous Heemskirk Granite, which is in close proximity. Consequently, in this short (30–60 Ma) interval between granite emplacement and tillite deposition, the granite body was exposed by erosion. The presently exposed crustal level of this granite was emplaced at a depth of 12–14 km (see discussion below). Thus this region was denuded, with corresponding uplift, by about ≤12–14 km during this period. The only deformational event recognised that may have occurred in this period is D_6 south over north thrusting and asymmetrical folding. This deformation may well be related to this significant period of uplift and denudation. Uplift may have been wholly the result of D_6 upthrusting, but was more plausibly due to isostatic rebound of the over-thickened crust that evolved during D_6 crustal shortening and thickening.

LATE CARBONIFEROUS TILLITE SEDIMENTATION

Scattered exposures of Zeehan Tillite are found throughout the Zeehan Quadrangle, particularly near the Eureka dolerite and on the plains immediately northeast of Zeehan. This diamictite consists of matrix-supported subrounded pebble-cobble clasts of mostly Oonah Formation quartzite, shale and quartz vein, and also clasts of granite, Crotty Sandstone and Dundas Group tuffs, within a grey muddy siltstone matrix. Correlation with other tillites of western Tasmania suggests a Late Carboniferous age for the Zeehan Tillite (Goscombe, 1991*a*).

D_7 DEFORMATION

The last fold event recognised (D_7) has expressions within the Oonah Formation, Ordovician–Devonian sequences, Heemskirk Granite and the Late Carboniferous Zeehan Tillite (Goscombe, 1991*a*) (fig. 1). D_7 is recognised in the Oonah Formation as upright open to closed NW-trending folds of metre to kilometre scale. The majority of these folds plunge 10–40° to the southeast. Crenulation cleavages trending 120–160° are fold axial planar to these folds and very common throughout the region. Fold axial planes and crenulation cleavages trend SE-NW and dip no more than 20° to the northeast or southwest. NW-trending crenulation cleavages are the last developed in the region, thus constraining the timing of this event. However these trends are identical to earlier D_3 tight folding, thus D_7 folds may in fact involve tightening of pre-existing folds in addition to the development of the pervasive D_7 crenulation cleavages and new, open, upright D_7 folds.

NW-trending upright folds are recognised in the Duck Creek Syncline. The earlier E-W folds were refolded into dome and basin interference patterns by this later folding (fig. 6). This second generation of folding has no penetrative planar cleavage developed but NW-trending mesoscopic kink bands are developed fold axial planar to the folds (fig. 1). The average width of these kink bands is 22 mm, and where developed they are spaced at 10–50 mm.

Two sets of NW-trending, spaced vertical cleavages are developed in the Late Carboniferous Zeehan Tillite. The average trends of these are 148° and 166°; these trends have been labelled D_{7a} and D_{7b} respectively. Bedding within the Zeehan Tillite, and in fact the overall shape of the main exposures of this tillite near Zeehan, is compatible with the tillite having been folded by NW-trending upright folds (Goscombe, 1991*a*).

Vertical to steeply southwest-inclined NW-trending shear zones are developed in the Heemskirk Granite (fig. 1). These are 300 mm wide zones of shear fabric development, grainsize reduction, and alignment of biotite laths and quartz-feldspar aggregate lenses. No sense of shear is apparent and no lateral displacement along the zones is recognised. There is no asymmetry within the zones; both margins grade equally with increasing fabric intensity towards the centre and have the appearance of being formed by pure shear. These shear zones may be associated

with the NE-trending shortening which gave rise to D_7 structures in the Oonah Formation and Zeehan Tillite.

All these D_7 structures are considered essentially coeval because of their coplanarity, late stage of development, and their generation by a SW-directed horizontal shortening axis. Consequently, D_7 deformation post-dates the Late Carboniferous Zeehan Tillite (Goscombe, 1991*a*). A post–Early Carboniferous age for D_7 is supported by zones of NE-SW shortening being recognised within the Heemskirk Granite. However, D_7 folding in the Zeehan Tillite did not involve significant shortening. This is in contrast with the open to closed D_7 folding and prevalent crenulation cleavage development in the Oonah Formation. Thus the bulk of D_7 folding and shortening may have occurred prior to deposition of the Zeehan Tillite, with minor tightening of these folds occurring subsequent to tillite deposition (Table 1). If this is so, the majority of D_7 strain could potentially have been synchronous with intrusion of the Heemskirk Granite. Such a scenario would explain the overall NW-trending elliptical shape of the pluton and ductile pure shear zones within the granite.

JURASSIC DOLERITE INTRUSION

The Eureka dolerite is mineralogically similar to known Jurassic dolerites from throughout Tasmania and is correlated with these (Spry, 1958). The elliptical shape of the Eureka dolerite is interpreted as being a cone sheet tapering downwards, i.e. synformal (Spry, 1958). Recent mapping has found Late Carboniferous Tillite exposures at the lower contact of the southeast portion of the intrusion (Goscombe, 1991*a*). Thus the dolerite may have intruded approximately into Late Carboniferous units. The shape of the cone sheet may well be controlled by a pre-existing NW-trending D_7 fold. However the presence of Oonah Formation in the centre of the cone sheet, with no tillite exposures recognised in this area, requires a less simplistic explanation. For example;

- was the Oonah Formation in the centre of the intrusion thrust over the tillite prior to dolerite intrusion?
- Or alternatively, is the cone sheet antiformal in shape?

UPLIFT PERIOD #3

A third stage of uplift, subsequent to dolerite intrusion and prior to deposition of Tertiary sediments on the resulting unconformity, is postulated. The region was uplifted and denuded exposing the Heemskirk Granite and Oonah Formation at approximately the crustal level presently exposed, this being accommodated by steeply-dipping normal faults. The nature of the tectonics that gave rise to the uplift and denudation of the granite and Oonah Formation prior to the Tertiary is not well documented. This event did not involve significant uplift and erosion as was experienced immediately after Heemskirk Granite emplacement (uplift period #2). This is because the Zeehan Tillite was not buried to any great degree, and dolerite intrusions in Tasmania, in general, were emplaced into extremely shallow crustal levels. Thus this third episode of uplift did not involved more than a few kilometres of movement.

TERTIARY SEDIMENTATION

A wide variety of Tertiary gravel, sand, clay, alluvial tin deposits, organic matter and boulder beds (including Heemskirk Granite clasts) were deposited during the Tertiary on the post-Carboniferous unconformity. A generalised Tertiary stratigraphy is recognised. The two basal units are recognised in most alluvial tin quarries, with sequences up to at least 6 m thick, but these units are of very limited distribution. The upper five units are recognised by mapping over the entire northwest portion of the Zeehan Quadrangle and are widely distributed.

(a) At the base are grey-green silt and mud and scattered wood and sand lenses. These are often sulphide rich and the wood is partially replaced by pyrite. They often contain high concentrations of tin;

(b) Non-indurated conglomerate consisting of claystone clasts within clay-rich sand;

(c) A blanket of fine to medium-grained clean sand covers a large portion of the area mapped. Vertical coal-filled cracks which trend 010° and 053° are found in Tertiary sands;

(d) These sands grade up into orange clay and sand immediately below basalt units. The clay often contains scattered, well-rounded, coarse, clear quartz grains;

(e) Extensive olivine basalt flows cover large areas, although they are not recognised in the general stratigraphy in all areas. Basalt is mostly weathered to orange clay with minor relict basalt nodules.

(e) Sands are rarely found on top of the basalt unit.

(f) The top of the sequence is typically the widely distributed gravel to cobble deposits, mostly with rounded clasts of Precambrian quartzite and quartz vein. These deposits are never seen on top of basalt and may in fact pre-date the basalt. This is supported by the cobble deposits near basalts being entirely silicified to a tough silicic conglomerate, possibly by hydrothermal fluids associated with the basalt flows.

UPLIFT PERIOD #4

A period of minor differential uplift after deposition of Tertiary sediments is inferred by the wide range in elevation of the base of the Tertiary sequences (fig. 1). The base of Tertiary deposits ranges from sea level to 210 m above sea level. The altitude of the Tertiary base increases stepwise inland from the coast, and so may be due to late-stage normal faulting of approximately NW-SE trends. Faults and joints in the Heemskirk Granite are of NW-SE trend, and NW-trending joints are dominant in the Eureka dolerite. Both may be related to this late-stage faulting and uplift.

HEEMSKIRK GRANITE CONTACT METAMORPHIC AUREOLE

PETROLOGY OF THE CONTACT AUREOLE

Assemblages developed in the contact metamorphic aureole are summarised in Table 2*a* and their locations presented in Figure 1. Although the bulk of the Oonah Formation rocks are variations on the theme of quartzite, thin (centimetre–metre scale) laminations/units of pelitic shale are scattered throughout the area. These pelites develop new mineral assemblages during contact metamorphism. All contact-metamorphosed pelites develop coarse laths of white to pale green micas (phengite), which are also developed in some quartzites. Biotite is developed in nearly all samples except black graphitic shale. Biotite is considered diagnostic of the limit of contact metamorphic effects because it is not developed in any sample of non-contact metamorphosed Oonah Formation (Table 2*b*), unlike phengite which is developed in both regionally and contact-metamorphosed Oonah Formation.

Cordierite is less commonly developed but is observable in the field (fig. 1). In thin section, cordierite is partially replaced, both internally and on the margins, by clusters of radiating needles of anthophyllite. These were presumably formed by hydrothermal retrogression during cooling after the contact metamorphic thermal pulse. In some samples, coarse anthophyllite appears to be in textural equilibrium with cordierite. Cordierite-bearing assemblages include cordierite-muscovite-biotite-quartz-anthophyllite.

Andalusite is commonly developed and easily recognisable in pelitic schist and black graphitic shale. Graphitic shales are black in outcrop and are aluminous and sulphurous, with muscovite-andalusite-quartz-graphite ± pyrite assemblages (Table 2*a*). These shales are conformable and tens of metres wide. Andalusite occurs as well-formed idioblastic crystals, shaped as blocks of chiastolite variety and also as needles. These are contained within a very fine-grained micaceous matrix containing muscovite, quartz and graphite. The margins of andalusite crystals are variably corroded by fine-grained muscovite ± biotite.

Contact-metamorphosed impure quartzites consist of fine to medium-grained, laths of chlorite, muscovite and biotite, with interstitial plagioclase and quartz. Fine tremolite and anthophyllite laths are also commonly present. Most samples contain minor amounts of yellow, green, brown or blue-green, fine tourmaline. Biotite is commonly orange and occurs as stubby laths that are not aligned. More schistose samples contain similar assemblages but lower modal proportions of quartz and more muscovite.

Sample 2536 is unique in the Heemskirk Granite aureole. This rock consists of coarse idioblastic garnet and tourmaline crystals in a biotite and chlorite-rich matrix. Also within this biotite-chlorite matrix are fine laths of green Ca-poor ferro-hornblende and clear anthophyllite. Tourmaline continued to grow during and subsequent to garnet growth (garnet growth presumably corresponds to the thermal peak), because garnet inclusions are found within tourmaline and tourmaline grows on the margins of garnet crystals (fig. 7). Tourmaline is predominantly blue to blue-green in thin section and highly zoned, with concentric rings of colour variation. Minor amounts of

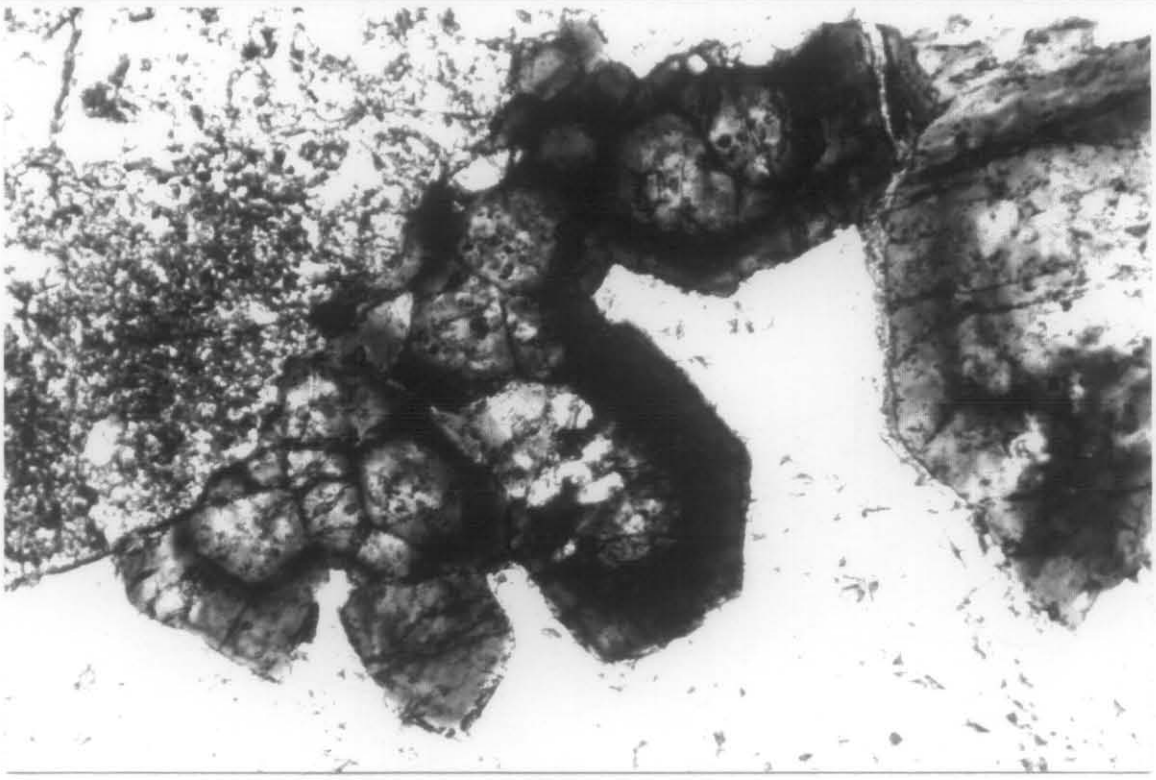

Figure 7.

Microphotograph, in plane polarised light, of late-stage zoned blue-green tourmaline on the margin of a garnet porphyroblast. Length of plate is 1.8 mm.

Table 2a

Summary of the petrology of contact-metamorphosed Oonah Formation, with approximate modal proportions.

Sample	and	cd	bi	mu	pl	kfd	q	chl	opaque	anth	tr	tm	graphite	hn	gn	Reactions
SPOTTED PELITES																
TH3		30	5	30			20		10	5						
1209		5	10	10			5			70						#4
1196*		26	40				15		4	15						#4
TH2		XPs	X	XR			X		X	XR						
404	15		10	20			50						5			#2
403A	5	<4	5	55			20	7	<4				<3			#1
SCHISTS																
387			X	X			X									
398	X		XR	X			X			X			X			
571				45			45				<3	<3				sphene
519A				40			50					10				
417				70		5	20	<4	<3		<4	<2	<3			#3
403B			X	X			X			X		X				
TH8				65			25		<5				<5			
2536*			35	<4			<4	25	<3	8		8		<5	15	#5,6,7
91-6			30	40			25	4				<2				
91-5	20			80												
TH9			X	X			X		X							
1195A			X	X		X	X		X	X			X	XR		
1018			3	47			40	8	2							
91-8			30			20	20		<4	10	20					
QUARTZITES and LAYERED QUARTZITES																
540							50			<2	20	30				
566							X		X		X	X				rutile
416				<5			50		<3		15	30				
303			X				X		X		X	X				
519B			X	X			X					X	X			
1008					30		55	<5								10% epi
1208A*			25	5	10	5	40	5		10	5					
91-9*			30				50	<5	<5	10		<3		5		
1206			20			5	75		<5							
1209E		5		20			68	5	<2			2				
BLACK SHALES																
442	5			20			30					<4	40			#1
521	5			20			30						45			#1
336	7			10			25						60			
91-3	10			30			30						30			#1

epi = epidote, bi = biotite, mu = muscovite, pl = plagioclase, kfd = K-feldspar, q = quartz, chl = chlorite, cc = calcite, anth = anthophyllite, tr = tremolite, tm = tourmaline, hn = hornblende, gn = garnet, and = andalusite, cd = cordierite. See Table 2b for explanation of other symbols.

chlorite and anthophyllite corrode the margins of garnet grains, thus these phases are at least in part retrogressive.

Comparison of these diverse contact aureole assemblages with experimental and theoretical phase stability relationships tightly constrain their formation to temperatures between 500–550°C (some samples formed at lower temperatures, this is the estimate for the maximum temperature attained) and pressures of 2–4 kbar (fig. 8). The maximum temperature limit is defined by the limit of quartz-chlorite stability, and the lower limit of T_{max} is constrained by the first formation of garnet. The maximum pressure is constrained by the limit of andalusite stability and the lower pressure limit by garnet stability (fig. 8). The presence of graphite in schist, as well as the black shale, is suggestive of reducing (low O_2 fugacity) conditions. This is supported by the presence of rutile in sample 566 (Table 2*a*).

MINERAL CHEMISTRY

All minerals were analysed using the Cameca SX50 electron microprobe in the central science laboratory at the University of Tasmania. Analysing conditions were by wavelength dispersive mode with an accelerating voltage of 20 kV and beam current of 20 nA (10 nA for micas) with magnification of 20 000 (10 000 for micas). Mineral analyses, for which cation proportions have been calculated using the program RECALC (Powell, pers. comm.), are contained in Appendix 1.

Cordierite in sample 1196 has an Fe/(Fe + Mg) ratio of 31% in the core and 28% in the rim. This is typical of

Table 2b

Summary of the petrology of regionally-metamorphosed Oonah Formation from the coastal section, with approximate modal proportions.

Sample	mu	pl	kfd	q	chl	cc	opaque	anth	tr	tm	pyrite	epidote
CALCAREOUS SCHISTS												
1090	50			35	<3	15	<3					
1092	5			80	<2	15	<2					
1094	50			30	8	12						
1095B	10			60		30	<2		<2	<2		
1113A		<4		5		90	5				<2	
1176	5	10		20	10	50					5	
1179	45			35	5	15	<3					
1096	10			20		70						
1173	5	47		10	5	30					3	
1113B		?5	5?	5		75	10					
SCHISTS												
1110A	60			15	25				<4			
1169C	80			5	15		<2					
1112	30			60	10		<2			<2		
91-7A	40			50	10		<2					
1176A	5			95								
91-10	55			40	5		<2					
91-11	57			30	10		3					
91-12	X			X	X		X					
MAFIC SCHISTS												
1168	35			45	20		<2			<2		
1168A	8	8		8	40	35						
1172*	<3	10		30	40	20	<3					
91-7	20			40	40							
1170	5	8		38	28	20	<3					
Nth outcrops	?	X		X	X				X			X

*	Minerals have been analysed for geothermobarometry.
X	Mineral present in matrix of sample.
Ps	Porphyroblast has been pseudomorphed.
R	Retrograde mineral.
reaction #1	Andalusite partly retrogressed by muscovite.
reaction #2	Andalusite partly retrogressed by muscovite and biotite.
reaction #3	Muscovite partly retrogressed by chlorite.
reaction #4	Cordierite partly retrogressed by anthophyllite ± muscovite
reaction #5	Anthophyllite partly retrogressed by blue-green hornblende.
reaction #6	Garnet partly retrogressed by anthophyllite.
reaction #7	Garnet partly retrogressed by chlorite.

contact metamorphic cordierite, although this cordierite is not as Fe-rich as those developed in the contact aureoles in northeast Tasmania (Goscombe *et al.*, 1992). There is no significant departure of the Al/Si ratio from the ideal of 4/5. TiO_2 is between 0.00–0.08%. K_2O, CaO, Na_2O and MnO are all insignificantly low, being 0.00–0.26%, 0.00%, 0.16–0.18% and 0.01% respectively. Fe_2O_3 contents are high, ranging 1.15–1.96%. Analysis totals are relatively high for cordierites (>98%), suggesting a low CO_2-H_2O volatile component in the structure.

Biotite Fe/(Fe + Mg) ratios are 23.9–24.1%, 46.7–46.8% and 27.27–28.51% for 1208A, 1196 and 91-9 respectively. The rims have the highest Fe/(Fe + Mg) ratios. All biotites have been recalculated assuming 15% of the Fe is Fe^{3+}. The Si/(Si + Al) ratios are 71%, 64% and 67% for 1208A, 1196 and 91-9 respectively. Biotite in 1208A is a phlogopite with high phlogopite component with respect to eastonite; 1196 is a biotite with a high eastonite-siderophyllite component; and 91-9 is a phlogopite with higher eastonite than phlogopite component (Deer *et al.*, 1966). TiO_2 contents range widely; 4.09–4.18% in 1208A, 1.84–2.06% in 1196, and 2.15 in 91-9. Na_2O and MnO are insignificantly low and CaO is absent.

Plagioclase in 1208A is of oligoclase composition; Ab = 73.5–76%, Or = 0.7–1.4% and An = 22–25%.

Garnet in 2536 is Mn-rich almanditic garnet of the following composition; almandine = 77.3%, pyrope = 7.5–9.2%, grossular = 7.4–7.8%, spessartine = 8.27–5.71% and andradite = 0.25–0.75%. Garnet inclusions within tourmaline are even more Ca and Mn-rich ($Alm_{72.5}$ Py_5 $Gross_{9.5}$ $Spess_{13}$ and $r_{0.25}$).

The blue and green tourmaline in 2536 is of a composition intermediate between dravite and schorl. Fe/(Fe + Mg) ratios are 38.6% in green tourmaline and 44–50% in blue tourmaline. All have Ca/(Ca + Na) ratios of 26–47%, the highest being in blue tourmaline rims. The green

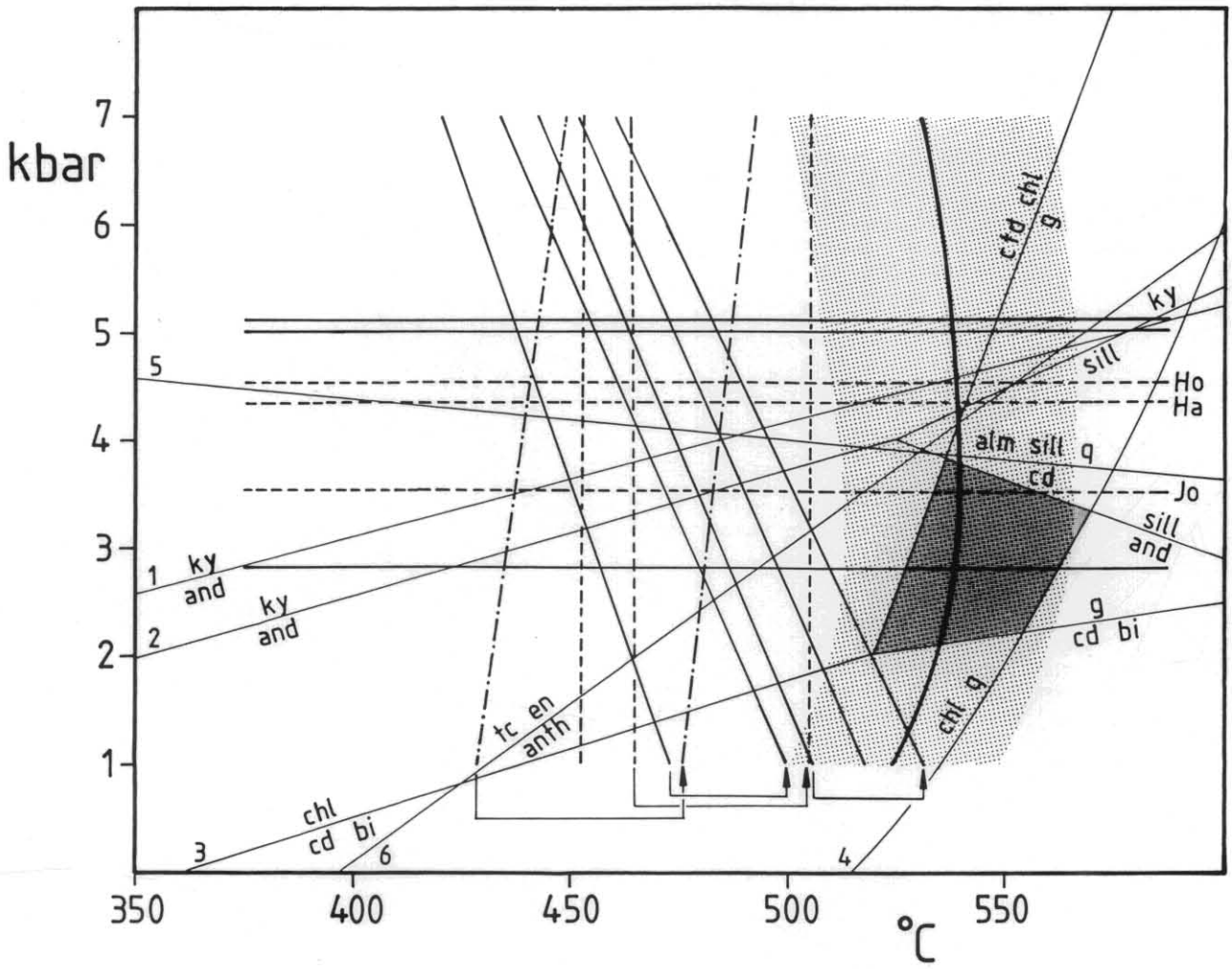

Figure 8.

Plots of geothermometer, equilibrium thermodynamics and geobarometer calculations for samples 1208A, 91-9 and 2536.

- solid thick line – Average T by equilibrium thermodynamics.
- light shaded region – Errors for equilibrium thermodynamics average T.
- solid thin line – Plagioclase-hornblende geothermometry (1208).
- vertical dashed line – Garnet-hornblende geothermometry (2536).
- dot-dashed line – Garnet-chlorite geothermometry (2536).
- arrows – From core to rim mineral pairs.
- solid horizontal line – Hornblende-chlorite geobarometry (2536).
- dash horizontal line – Hornblende geobarometry (2536) labelled by abbreviation of the author of relevant calibration.

Numbered thin lines are published experimental and theoretically-calculated phase equilibria for pelitic systems. Dark shaded region is the best constrained stability field of contact aureole assemblages from adjacent to the Heemskirk Granite.

(1) Aluminosilicate stability (Richardson *et al.*, 1969).

(2) Aluminosilicate stability (Holdaway, 1971).

(3) Theoretically calculated equilibria in KFASH (Powell and Holland, 1990).

(4) Experimental limit of chlorite-quartz stability (see Massone, 1989).

(5) Experimental and theoretical equilibria in FASH (Bickle and Archibald, 1984).

(6) Theoretically calculated equilibria in MASH (Day *et al.*, 1985).

See Table 2 for mineral abbreviations. In addition; tc = talc, en = enstatite, ky = kyanite, sill = sillimanite, g = garnet, ctd = chloritoid, alm = almandine garnet.

tourmaline is relatively Al-rich and so has a minor component of elbaite end member (which is absent from blue tourmaline) of approximately 10%. Tourmaline in sample 91-9 is of dravite composition with significant schorl component, with Fe/(Fe + Mg) ratios ranging from 34.8% in the core to 37.2% in the rim. Uvite component is also significant, with Ca/(Ca + Na) ratios of 36.2% in the core to 49.6% in the rim. This tourmaline has no elbaite component. All tourmalines have analysis totals of 13–14% below 100%. This deficit is taken up by typical values of 10% B_2O_3 and <4% H_2O (Deer *et al.*, 1966). Thus these tourmalines are thought not to contain lithium.

Chlorite in 1208A is Fe-poor ripidolite (Deer *et al.*, 1966) with Fe + Fe^{3+}/(Fe + Fe^{3+} + Mg) ratio of 25.6%, no CaO or MnO, and only 1.74% TiO_2. Chlorite in 91-9 is ripidolite with Fe + Fe^{3+}/(Fe + Fe^{3+} + Mg) ratios of 39.1–39.5%, insignificant CaO, 0.06–0.10% TiO_2 and 0.09–0.15% MnO. Chlorites in 2536 are Fe-rich ripidolites with Fe + Fe^{3+}/(Fe + Fe^{3+} + Mg) ratios of 52.2–53.6% and no CaO, low TiO_2 (0.00–0.10%), and significant MnO contents (0.01–0.19%).

Three amphibole types (Leake, 1978) are recognised in these samples; ferro-hornblende and anthophyllite in 2536, anthophyllite only in 1196, and tremolite and anthophyllite in 1208A. The ferro-hornblende in 2536 has low CaO contents (5.3–5.5%) and so is on the border of hornblende compositions. This ferro-hornblende has Fe/(Fe + Mg) ratios of 60–63% and Al-cations of 1.65–2.52 (for 24 oxygen). Ti contents were 0.02 cations, which is typical of low-grade hornblendes (Raase, 1974). Anthophyllite in samples 2536, 1196 and 1208A had Fe/(Fe + Mg) ratios of 55%, 46% and 25% respectively. The anthophyllites in 2536 and 1208A had significant CaO (0.78–3.41%) contents and low Na_2O (0.07–0.16%) and K_2O (0.00–0.02%) contents. Sample 1196, retrograde anthophyllite after cordierite, had low CaO (0.14%) and (0.06%), Na_2O and no K_2O. Tremolite in sample 1208A had low Fe/(Fe + Mg) ratios, ranging from 15.2–16.2% and averaging 15.6%. Most of these tremolites have typical CaO contents (11.5–11.8%) but one is Ca-poor (8%) and slightly more Fe-rich (Fe/(Fe + Mg) = 19.3%).

Sample 1172 is the only sample of regionally metamorphosed Oonah Formation for which there is a mineral analysis. Only muscovite was analysed; this had an Fe/(Fe + Mg) ratio of 25.6%, and was recalculated assuming 60% of all Fe is Fe^{3+}. The paragonite component was low, the Na/(Na + K) ratio being 5.6%. CaO was absent and MnO insignificantly low (0.03%). The TiO_2 content was 0.24%, and the Si cation content, based on 12 oxygen,was 3.28. The Si in phengite geobarometer (Massone and Schreyer, 1987) applied to this sample gives rise to pressures of 5250–6450 bar over a temperature estimate range of 300–400°C.

GEOTHERMOMETRY

The garnet-chlorite (Grambling, 1990) and garnet-hornblende (Graham and Powell, 1984) geothermometers were applied to sample 2536 (Table 3). The results ranged from 436–486°C and 452–505°C respectively, for a pressure estimate of 4.5 kbar. The hornblende-plagioclase (Blundy and Holland, 1990) geothermometer was applied to sample 1208A with results of 451–501°C, for a pressure estimate of 4.5 kbar (Table 4). These results are remarkably consistent with each other and are thus considered real T estimates.

Furthermore, all samples consistently show rims equilibrated at higher temperatures (486–505°C) than the cores (436–470°C) (fig. 8). This suggests progressive mineral growth during the thermal pulse, with mineral growth culminating at the thermal peak. The preservation of such a trend suggests that these mineral pairs have not re-equilibrated during cooling. Consequently these temperatures can be considered real, given that the respective geothermometers have been calibrated correctly. However these results are 30–80°C lower than temperature estimates by equilibrium thermodynamics and phase stability constraints (fig. 8).

The maximum temperature experienced in the contact aureole (for the samples used) is in the order of 505°C based on geothermometry, and 535°C based on equilibrium thermodynamics. These temperatures of

Table 3

Garnet-chlorite (Grambling, 1990) and garnet-hornblende (Graham & Powell, 1984) geothermometry in sample 2536, in °C.

			Garnet-chlorite		Garnet-hornblende	
Garnet	Chlorite	Hornblende	$P_{est.}$ (kbar)	T result	$T_{est.}$ (°C)	T result
c4core	c4	c4	2	429	300	472
			3	432	400	468
			4	435	500	464
c4rim	c4	c4	2	479	300	514
			3	481	400	509
			4	484	500	505
c4core	c4 in gn		2	432		
			3	435		
			4	438		

Table 4

Hornblende-plagioclase (Blundy and Holland, 1990) and biotite-chlorite (Dickenson, *in* Laird, 1989) geothermometry in sample 1208A, in °C.

Hornblende	Plagioclase	Biotite	Chlorite	$P_{est.}$ (kbar)	Horn-Plag T result	Bio-Chl T result
c1#1	c1core	c1core	c1	2	496	371
				3	485	378
				4	474	386
c1#2	c1rim	c1rim	c1	2	519	381
				3	507	389
				4	496	396
c5#1	c2core	c6core	c1	2	467	360
				3	457	367
				4	446	374
c5#2	c2rim			2	489	
				3	478	
				4	467	
c6#2	c6core			2	507	
				3	496	
				4	485	

contact metamorphism are very low compared to contact aureoles around granitoids from the literature, which are typically in the order of 600–650°C (Goscombe *et al.*, 1992). Consequently, the intruding Heemskirk Granite must have been a relatively cool granite body at the time of emplacement.

Additional geothermometers were applied, these giving either geologically unreasonable results or significantly lower temperatures. The biotite-chlorite geothermometer (Dickenson, *in* Laird, 1989) applied to sample 1208A gave results of 360–390°C, which is 80–90°C lower than the other calibrations. In my experience this calibration is typically 50–150°C lower than the garnet-biotite (Ferry and Spear, 1978) geothermometer results from the same rocks. In addition to the low calibration of this method, these results may be low because chlorite may be a retrogressive phase and not in equilibrium with the biotite.

The biotite-tourmaline (Colopietro and Frieberg, 1987) geothermometer applied to sample 91-9 gave low temperatures (360–375°C). The biotite and tourmaline may not be in equilibrium; tourmaline may have crystallised at a slightly later stage during hydrothermal alteration immediately after the peak of the thermal pulse.

EQUILIBRIUM THERMODYNAMICS

Equilibrium thermodynamics by the method of Powell and Holland (1985, 1988) was applied to one suitable sample (2536) for average temperature calculations. All calculations were performed using the program THERMOCALC v2.01β (Powell and Holland, pers. comm., 1992) with the most up-to-date thermodynamic dataset (1992). For the equilibrium assemblage garnet-chlorite-hornblende-quartz-anthophyllite, the following independent reactions involving the relevant mineral end members can be drawn up.

(1) 7ames + 2anth + 12q = 14py + 30H_2O

(2) 9ames + 6hb + 12q = 20py + 4gr + 42H_2O

(3) 3ames + 6hb + 3parg = 11py + 4gr + 3ed + 18H_2O

(4) 27ames + 24hb + 6gl = 58py + 8gr + 12 parg + 126H_2O

[ames = amesite, anth = anthophyllite, q = quartz, py = pyrope, hb = hornblende, gr = grossular, parg = pargasite, ed = edenite, gl = glauconite]

The results of the average temperature calculations, using these reactions, the mineral activities calculated from the mineral analyses, and the thermodynamic dataset, are tabulated below and are plotted in Figure 8.

Pressure est. (kbar)	1	2	3	4	5	6	7
Ave. temp. (°C)	524	535	538	538	537	534	531
sd (error in °C)	23	25	27	27	28	29	31
f (<1.61 for 95% confidence)	0.9	0.9	0.9	0.9	1.0	1.0	1.1

These results are approximately 30–60°C higher than estimates from the same sample by conventional geothermometry. The error and statistical fit of the average temperature result is very good and the results closely correspond to phase stability constraints (fig. 8). Consequently the equilibrium thermodynamics average temperature is considered a reliable maximum temperature (T_{max}) for the Heemskirk thermal aureole.

GEOBAROMETRY

No reliable geobarometry has been performed on the Heemskirk contact aureole for want of suitable assemblages. The most reliable pressure estimate is ≤4.5 kbar as defined by the upper pressure stability of

andalusite (fig. 8). A pressure estimate for the emplacement of the Heemskirk Granite is possibly as high as 4.5 kbar, as suggested by the following tentative results.

The aluminium in hornblende geobarometer was applied to the hornblende in sample 2536. This rock sample, being pelitic, is far more aluminous than the granodiorite compositions with which this geobarometer was calibrated, and consequently inappropriate for this sample. However the results are consistent with the upper pressure limit of andalusite; the results being 4546, 4380 and 3520 kbar for Hollister *et al.* (1987), Hammarstrom and Zen (1986), and Johnson and Rutherford (1989) calibrations respectively. Similarly, the hornblende-chlorite geobarometer (Moonsup Cho, *in* Laird, 1989) yielded a wide spread of results centred on the upper limiting pressure for andalusite. The results from sample 2536 are 5128, 5029, 5028 and 2819 kbar.

Although none of the above pressure constraints are individually reliable, their broad consistency with each other supports a preferred pressure of 3500–4000 kbar at the time of emplacement of the Heemskirk Granite. Further work involving pressure estimates by the phengite geobarometer (Massone and Schreyer, 1987) may yield reasonable results if the temperature of equilibration is accurately and confidently known for the same sample (Goscombe *et al.*, 1992).

IMPLICATIONS OF HEEMSKIRK GRANITE CONTACT AUREOLE CONDITIONS

The Oonah Formation was contact metamorphosed by the Heemskirk Granite to a maximum temperature of 490–535°C, while residing at approximately 3500–4000 kbar. Such low contact aureole temperatures suggest that the Heemskirk Granite was a relatively cool granite body at the time of emplacement (Goscombe *et al.*, 1992), as is suggested by the narrow thermal aureole (1–2 km). This may be the result of the granite magma partially solidifying and cooling as it rose through the crust from much lower crustal levels.

The preferred estimate of crustal pressure at the time of emplacement suggests a depth of burial of approximately 12–14 km (Winkler, 1979). Thus 12–14 km of upper crust was eroded with accompanying uplift in the 30–60 Ma period between granite emplacement (347–351 Ma) and deposition of the Zeehan Tillite, which contains granite clasts, in the Late Carboniferous (320–280 Ma). This second period of uplift (Table 1) is a significant tectonic event and may be the result of either of the following scenarios.

(1) Isostatic uplift in response to crustal over-thickening that resulted from D_6 folding and crustal shortening.

(2) Alternatively, uplift may be due entirely to upthrusting associated with N-S directed shortening and south over north thrusting during the D_6 deformational period.

CONCLUSIONS

(1) Regional metamorphism of the Oonah Formation occurred during the first recognised deformational event (D_1); all subsequent deformational events occurred at lower metamorphic grade. The grade of regional metamorphism increases from sub-greenschist facies in the majority of the mapped region in the south, to greenschist facies in the very northwest corner of the Zeehan Quadrangle. The highest metamorphic grades are indicated by tremolite-plagioclase-quartz-epidote assemblages. For typical greenschist facies temperatures of 300–400°C, a pressure estimate of 5250–6450 bar is suggested by one phengite geobarometer result from sample 1172 in the most northerly exposures of Oonah Formation in the quadrangle. These pressures suggest that approximately 18–22 km of uplift and denudation were experienced subsequent to D_1 and prior to deposition of the Ordovician–Devonian sequences. Four major tight to open fold events (D_2–D_5) occurred in this period; thus it can be confidently assumed that western Tasmania experienced crustal shortening and concomitant crustal thickening at this time. The most geologically plausible explanation for such a large component of denudation is by late-stage isostatic rebound in response to crustal over-thickening during D_2–D_5.

(2) The first deformational event recognised involved isoclinal folding with an intense axial planar foliation of aligned micas and quartz aggregate ribbons (S_1). This intense foliation is correlated with the ubiquitous pervasive foliation developed subparallel (i.e. <10°) with bedding in all outcrops of Oonah Formation. This deformational event was undoubtedly early formed and may even be unique to the Oonah Formation. Thus the presence of a pervasive bedding-parallel foliation offers a reliable and field-practical definition of what constitutes the Oonah Formation. It must be noted that intense penetrative planar foliations are also developed in the younger sequences of western Tasmania (i.e. Eocambrian and Cambrian). These may be planar foliation equivalents to crenulation cleavages and they may be at a high angle to bedding. Thus it is felt that the must important distinguishing criteria of the S_1 fabric is that it is invariably parallel to subparallel to bedding. This is in contrast to previous definitions of the Oonah Formation. For example:

   (a) Brown (1986) defines the Oonah Formation by the presence of isoclinally-refolded isoclines. Isoclines are very rare in inland outcrops and not common in the coastal section, where there is continuous outcrop. Thus the scarcity of isoclines, let alone isoclinally-refolded isoclines, does not lend their presence or absence to being a very practical field criteria for what constitutes the Oonah Formation.

   (b) Similarly, the presence of a crenulation cleavage trend in the Oonah Formation, but not in younger (Eocambrian–Devonian) sequences, does not prove to be a practical definition for the Oonah Formation. This is because such a multitude of crenulation trends are recognised in Eocambrian

to Devonian sequences (E-W, NE-SW, N-S and NW-SE: Brown, 1986; Seymour, 1981; Williams and Turner, 1974) that no additional trend can be confidently correlated with development in the Oonah Formation only. Similarly, defining the Oonah Formation by the number of crenulation cleavages developed with respect to younger sequences is impractical in the field because the spatial distribution of each crenulation generation is not homogeneous across the region.

(3) Subsequent to D_1 folding and fabric development, two tight and inclined fold events (D_2–D_3) and two upright open to tight fold events (D_4–D_5) are recognised in the Oonah Formation. These events are not recognised in the Ordovician–Devonian sequences of the Duck Creek Syncline. Consequently these deformation events may be Precambrian or Cambrian in age.

(4) D_6 deformation involved south over north, high angle thrusting and asymmetrical east-trending folding. This event is recognised in the Ordovician–Devonian sequences but not in the Late Carboniferous Zeehan Tillite, thus this deformation may be of Early Carboniferous age. Expressions of D_6 deformation are not recognised in the Heemskirk Granite, this however does not negate D_6 deformation post-dating this granite. This deformation may be responsible for the postulated 12–14 km of uplift and denudation experienced by the region subsequent to Heemskirk Granite emplacement. This uplift occurred prior to deposition of the Late Carboniferous Zeehan Tillite and so is tightly constrained to occurring in the 347–320 Ma interval. This is a very short period of time for a significant component of denudation, thus this uplift must be considered a major tectonic event.

(5) The low maximum temperatures (450–535°C) recorded in the Heemskirk Granite thermal aureole suggest that this granite was emplaced as a low temperature and possibly partly solidified pluton. At a late stage of crystallisation a boron and silica-rich fluid was pumped into the surrounding Oonah Formation. This haloe of hydrothermal alteration was irregular in shape and possibly largely controlled by pre-existing faults and fractures. Thus a NW-trending 'apophysis' of this aureole suggests that the NW-SE fault trend existed prior to granite emplacement.

FURTHER WORK

A more detailed metamorphic study of the contact aureole is needed to confidently constrain the depth of granite emplacement. Suggested geobarometers that may be applicable are the phengite (Massone and Schreyer, 1987), biotite–K-feldspar–muscovite and biotite-muscovite-chlorite (Powell and Evans, 1983; Bucher-Nurminen, 1987) geobarometers, and possibly hornblende geobarometry if hornblende is found in the granite. The biotite-muscovite geothermometer (Hoisch, 1989) can be applied to appropriate pelitic assemblages.

A more detailed study of the Precambrian D_1 metamorphism is required. The increase in metamorphic grade to the north needs to be tested and quantitatively constrained with illite crystallinity (see *Journal of Metamorphic Geology*, volume 9 (6), 1991), calcite-dolomite (see collation in Dachs, 1990), chlorite (Cathelineau, 1988) and hornblende-plagioclase (Spear, 1981; Blundy and Holland, 1990) geothermometry and phengite geobarometry (Massone and Schreyer, 1987).

The first and second uplift events are significant tectonic events for which the stress fields and nature of tectonics are unknown. An analysis of the timing relationships of faulting and thrusting in western Tasmania is required. Combined with this information should be an analysis of shear sense along slickenlines in large populations of faults of known ages, to define the stress field by the method of Will and Powell (1991). This information may lead to a better understanding of the tectonics at the time of these uplift periods.

REFERENCES

BICKLE, M. J.; ARCHIBALD, N. J. 1984. Chloritoid and staurolite stability: implications for metamorphism in the Archaean Yilgarn Block, Western Australia. *Journal Metamorphic Geology*. 2:179–203.

BLUNDY, J. D.; HOLLAND, T. J. B. 1990. Calcic amphibole equilibria and a new amphibole-plagioclase geothermometer. *Contributions Mineralogy and Petrology*. 104:208–224.

BROOKS, C.; COMPSTON, W. 1965. The age and initial Sr^{87}/Sr^{86} of the Heemskirk Granite, western Tasmania. *Journal Geophysical Research*. 70:6249–6262.

BROWN, A. V. 1986. Geology of the Dundas–Mt Lindsay–Mt Youngbuck region. *Bulletin Geological Survey Tasmania*. 62.

BUCHER-NURMINEN, K. 1987. A recalibration of the chlorite-biotite-muscovite geobarometer. *Contributions Mineralogy and Petrology*. 96:519–522.

CATHELINEAU, M. 1988. Cation site occupancy in chlorites and illites as a function of temperature. *Clay Minerals*. 23:471–485.

COLOPIETRO, M. R.; FRIBERG, L. M. 1987. Tourmaline-biotite as a potential geothermometer for metapelites, Black Hills, South Dakota. *Abstracts with Programs Geological Society of America*. 19:624.

DACHS, E. 1990. Geothermobarometry in metasediments of the southern Grossvenediger area (Tauern Window, Austria). *Journal Metamorphic Geology*. 8:217–230.

DAY, H. W.; CHERNOSKY, J. V.; KUMIN, H. J. 1985. Equilibria in the system MgO-SiO_2-H_2O: a thermodynamic analysis. *American Mineralogist*. 70:237–248.

DEER, W. A.; HOWIE, R. A.; ZUSSMAN, J. 1966. *An introduction to the rock forming minerals*. Longman : London.

FERRY, J. M.; SPEAR, F. S. 1978. Experimental calibration of the partitioning of Fe and Mg between biotite and garnet. *Contributions Mineralogy and Petrology*. 66:113–117.

FINDLAY, R. H.; BROWN, A. V. 1992. The 10th Legion Thrust, Zeehan District. Distribution, interpretation, and regional and economic significance. *Report Division of Mines and Mineral Resources Tasmania*. 1992/02.

GOSCOMBE, B. D. 1991*a*. Deformation of the Zeehan Tillite and re-evaluation of the Tabberabberan Orogeny. *Report Division of Mines and Mineral Resources Tasmania*. 1991/03.

GOSCOMBE, B. D. 1991*b*. Intense non-coaxial shear and the development of mega-scale sheath folds in the Arunta Block, Central Australia. *Journal Structural Geology*. 13:299–318.

GOSCOMBE, B. D.; MCCLENAGHAN, M. P.; EVERARD, J. E. 1992. Contact metamorphism of the Mathinna Beds and the depth of crustal residence during mega-kinking in northeast Tasmania. *Report Department of Mines Tasmania*. 1992/34.

GRAHAM, C. M.; POWELL, R. 1984. A garnet-hornblende geothermometer: calibration, testing and application to the Pelona Schist, Southern California. *Journal Metamorphic Geology*. 2:13–31.

GRAMBLING, J. A. 1990. Internally-consistent geothermometry and H_2O barometry in metamorphic rocks: the example garnet-chlorite-quartz. *Contributions Mineralogy and Petrology*. 105:617–628.

HAMMARSTROM, J. M.; ZEN, E-AN. 1986. Aluminium in hornblende: an empirical igneous geobarometer. *American Mineralogist*. 71:1297–1313.

HOISCH, T. D. 1989. A muscovite-biotite geothermometer. *American Mineralogist*. 74:565–572.

HOLDAWAY, M. J. 1971. Stability of andalusite and the aluminum-silicate phase diagram. *American Journal of Science*. 271:97–131.

HOLLISTER, L. S.; GRISSOM, G. C.; PETERS, E. K.; STOWELL, H. H.; SISSON, V. B. 1987. Confirmation of the empirical correlation of Al in hornblende with pressure of solidification of calc-alkaline plutons. *American Mineralogist*. 72:231–239.

JOHNSON, M. C.; RUTHERFORD, M. J. 1989. Experimental calibration of the aluminum-in-hornblende geobarometer with application to Long Valley caldera (California) volcanic rocks. *Geology*. 17:837–841.

LAIRD, J. 1989. Chlorites: metamorphic petrology. *Reviews in mineralogy*. 19:405–453.

LEAKE, B. E. 1978. Nomenclature of amphiboles. *Mineralogical Magazine*. 42:533–563.

MASSONE, H. -J. 1989. The upper thermal stability of chlorite + quartz: an experimental study in the system MgO-Al_2O_3-SiO_2-H_2O. *Journal Metamorphic Geology*. 7:567–581.

MASSONNE, H. -J.; SCHREYER, W. 1987. Phengite geobarometry based on the limiting assemblage with K-feldspar, phlogopite and quartz. *Contributions Mineralogy and Petrology*. 96:212–224.

POWELL, R.; EVANS, J. A. 1983. A new geobarometer for the assemblage biotite-muscovite-chlorite-quartz. *Journal Metamorphic Geology*. 1:331–336.

POWELL, R.; HOLLAND, T. J. B. 1985. An internally consistent thermodynamic dataset with uncertainties and correlations: 1. Methods and a worked example. *Journal Metamorphic Geology*. 3:327–342.

POWELL, R.; HOLLAND, T. J. B. 1988. An internally consistent dataset with uncertainties and correlations: 3. Applications to geobarometry, worked examples and a computer program. *Journal Metamorphic Geology*. 6:173–204.

POWELL, R.; HOLLAND, T. J. B. 1990. Calculated mineral equilibria in the pelite system, KFMASH (K_2O-FeO-MgO-Al_2O_3-SiO_2-H_2O). *American Mineralogist*. 75:367–380.

RAASE, P. 1974. Al and Ti contents of hornblende, indicators of pressure and temperature of regional metamorphism. *Contributions Mineralogy and Petrology*. 45:231–236.

RICHARDSON, S. W.; GILBERT, M. C.; BELL, P. M. 1969. Experimental determination of kyanite-andalusite and andalusite-sillimanite equilibria; the aluminum silicate triple point. *American Journal of Science*. 267:259–272.

SEYMOUR, D. B. 1981. *The Tabberabberan Orogeny in northwest Tasmania*. Ph.D. Thesis, University of Tasmania.

SPEAR, F. S. 1981. An experimental study of hornblende stability and compositional variability in amphibolite. *American Journal of Science*. 281:697–734.

SPRY, A. 1958. Some observations of the Jurassic dolerite of the Eureka cone sheet near Zeehan, Tasmania, *in: Dolerite: a symposium*. 93–129. Geology Department, University of Tasmania.

WILL, T. M.; POWELL, R. 1991. A robust approach to the calculation of paleostress fields from fault plane data. *Journal Structural Geology*. 13:813–821.

WILLIAMS, E.; TURNER, N. J. 1974. Geological atlas 1:250 000 series. Sheet SK–55/3. Burnie. *Explanatory Report Geological Survey Tasmania*.

WINKLER, H. G. F. 1979. *Petrogenesis of metamorphic rocks (5th edition)*. Springer-Verlag.

[26 October 1993]

APPENDIX 1

Mineral analyses

Mineral analyses from contact metamorphosed Oonah Formation adjacent to the Heemskirk Granite. Sample 1172 is from regionally metamorphosed Oonah Formation. Each analysis is labled by the circle on the thin section that the analysis is from (i.e. c1#2 denotes second analysis in circle 1). Electron microprobe conditions and recalculation method are discussed in the text. A dash denotes where element was not analysed, or alternatively is not applicable.

	trem 1208 c1#1	trem 1208 c1#2	trem 1208 c5#1	trem 1208 c5#2	trem 1208 c6#2	anth 1208 c1#3	anth 1208 c6#1	bi 1208 c1core	bi 1208 c1rim	bi 1208 c6core
SiO_2	54.92	54.35	55.23	54.83	54.51	55.04	56.04	39.07	38.83	39.59
TiO_2	0.39	0.51	0.32	0.43	0.45	0.17	0.14	4.13	4.18	4.09
Cr_2O_3	0.00	0.00	0.02	0.00	0.02	0.06	0.01	0.00	0.00	0.00
Al_2O_3	2.01	2.31	1.36	1.82	2.14	1.00	0.48	13.19	13.25	13.65
Fe_2O_3	1.28	1.32	1.75	1.26	1.26	2.45	2.66	1.93	1.92	1.93
FeO	6.52	6.75	8.91	6.43	6.45	12.49	13.57	9.86	9.80	9.83
MnO	0.21	0.25	0.52	0.30	0.29	0.67	0.49	0.07	0.06	0.00
MgO	19.75	19.74	20.89	19.94	19.87	21.52	22.92	17.44	17.29	17.43
CaO	11.77	11.60	8.08	11.51	11.64	3.41	1.14	0.00	0.01	0.01
Na_2O	0.36	0.41	0.15	0.20	0.22	0.12	0.07	0.23	0.25	0.25
K_2O	0.11	0.11	0.05	0.07	0.10	0.02	0.01	9.53	9.24	9.48
H_2O	2.13	2.13	2.13	2.12	2.12	2.11	2.13	4.10	4.08	4.15
Total	99.45	99.48	99.40	98.90	99.07	99.06	99.66	99.55	98.88	100.40
Si	7.72	7.66	7.78	7.74	7.70	7.82	7.89	2.86	2.85	2.86
Ti	0.04	0.05	0.03	0.05	0.05	0.02	0.01	0.23	0.23	0.22
Cr	0.00	0.00	0.00	0.00	0.00	0.01	0.00	0.00	0.00	0.00
Al	0.33	0.38	0.23	0.30	0.36	0.17	0.08	1.14	1.15	1.16
Fe^{3+}	0.14	0.14	0.19	0.13	0.13	0.26	0.28	0.11	0.11	0.10
Fe^{2+}	0.77	0.80	1.05	0.76	0.76	1.48	1.60	0.60	0.60	0.59
Mn	0.02	0.03	0.06	0.04	0.03	0.08	0.06	0.00	0.00	0.00
Mg	4.14	4.14	4.39	4.20	4.18	4.56	4.81	1.90	1.89	1.88
Ca	1.77	1.75	1.22	1.74	1.76	0.52	0.17	0.00	0.00	0.00
Na	0.10	0.11	0.04	0.05	0.06	0.03	0.02	0.03	0.04	0.03
K	0.02	0.02	0.01	0.01	0.02	0.00	0.00	0.89	0.87	0.87
OH	2.00	2.00	2.00	2.00	2.00	2.00	2.00	2.00	2.00	2.00

	chlor 1208 c1	plag 1208 c1core	plag 1208 c1rim	plag 1208 c2core	plag 1208 c2rim	plag 1208 c6core	cord 1196 core	cord 1196 rim	bio 1196 #1	bio 1196 #2
SiO_2	28.33	61.59	62.12	62.92	61.88	61.62	48.39	48.07	35.33	35.67
TiO_2	1.74	0.00	0.01	0.00	0.00	0.02	0.00	0.08	2.06	1.84
Cr_2O_3	0.04	0.02	0.00	0.00	0.02	0.00	0.00	0.00	0.00	0.00
Al_2O_3	19.76	22.71	23.10	22.55	23.02	23.29	32.85	32.25	16.69	16.88
Fe_2O_3	2.41	-	-	-	-	-	1.15	1.96	3.40	3.45
FeO	12.29	0.09	0.09	0.14	0.13	0.15	6.90	6.11	17.34	17.61
MnO	0.06	0.01	0.00	0.04	0.03	0.00	0.14	0.12	0.06	0.00
MgO	23.68	0.00	0.00	0.00	0.02	0.00	8.79	9.03	11.10	11.33
CaO	0.04	5.13	5.12	4.48	5.04	5.44	0.03	0.03	0.00	0.02
Na_2O	0.00	8.28	8.32	8.53	8.10	7.92	0.16	0.18	0.49	0.45
K_2O	0.00	0.12	0.15	0.24	0.19	0.14	0.00	0.26	8.35	8.29
SrO	-	0.25	0.22	0.21	0.26	0.24	-	-	-	-
BaO	-	0.00	0.01	0.02	0.00	0.00	-	-	-	-
H_2O	12.22	-	-	-	-	-	-	-	3.93	3.96
Total	100.56	98.20	99.15	99.14	98.67	98.81	98.41	98.08	98.76	99.51
Si	2.78	2.78	2.78	2.81	2.78	2.76	4.97	4.96	2.70	2.70
Ti	0.13	0.00	0.00	0.00	0.00	0.00	0.00	0.01	0.12	0.11
Cr	0.00	0.00	0.00	0.00	0.00	0.00	0.00	0.00	0.00	0.00
Al	2.29	1.21	1.22	1.19	1.22	1.23	3.98	3.92	1.50	1.51
Fe^{3+}	0.18	-	-	-	-	-	0.09	0.15	0.20	0.20
Fe^{2+}	1.01	0.00	0.00	0.01	0.00	0.01	0.59	0.53	1.11	1.12
Mn	0.00	0.00	0.00	0.00	0.00	0.00	0.01	0.01	0.00	0.00
Mg	3.46	0.00	0.00	0.00	0.00	0.00	1.34	1.39	1.26	1.28
Ca	0.00	0.25	0.25	0.21	0.24	0.26	0.00	0.00	0.00	0.00
Na	0.00	0.73	0.72	0.74	0.71	0.69	0.03	0.04	0.07	0.07
K	0.00	0.01	0.01	0.01	0.01	0.01	0.00	0.03	0.81	0.80
Sr	-	0.01	0.01	0.01	0.01	0.01	-	-	-	-
Ba	-	0.00	0.00	0.00	0.00	0.00	-	-	-	-
OH	8.00	-	-	-	-	-	-	-	2.00	2.00

	anth 1196	bio 91-9 c2core	bio 91-9 c2rim	bio 91-9 c2#2	chlor 91-9 c1core	chlor 91-9 c1rim	tourm 91-9 core	tourm 91-9 rim	musc 1172	horn 2536 c4
SiO_2	52.72	38.06	38.44	38.58	26.49	26.95	36.35	36.39	49.35	44.08
TiO_2	0.04	2.15	2.13	2.09	0.06	0.10	0.52	1.17	0.24	0.15
Cr_2O_3	0.00	0.00	0.00	0.00	0.00	0.00	0.04	0.03	0.00	0.02
Al_2O_3	1.17	15.69	15.56	15.97	20.52	20.60	28.76	26.90	28.60	8.99
Fe_2O_3	4.54	2.23	2.29	2.24	3.69	3.70	-	-	3.08	4.31
FeO	23.13	11.35	11.69	11.45	18.81	18.86	8.35	9.51	1.85	21.98
MnO	0.51	0.10	0.06	0.17	0.09	0.15	0.06	0.09	0.03	0.68
MgO	15.40	16.89	16.35	16.90	18.91	19.40	8.79	9.00	2.91	8.15
CaO	0.14	0.00	0.00	0.00	0.02	0.03	1.70	2.58	0.00	5.53
Na_2O	0.06	0.22	0.13	0.15	0.00	0.00	1.66	1.45	0.39	1.00
K_2O	0.00	9.02	9.33	9.17	0.00	0.00	0.13	0.02	9.94	0.23
H_2O	2.03	4.10	4.10	4.14	11.78	11.95	-	-	4.52	1.92
Total	99.74	99.81	100.08	100.87	100.38	101.74	86.40	87.15	100.89	97.04
Si	7.79	2.79	2.81	2.79	2.70	2.70	5.89	5.91	3.28	6.88
Ti	0.00	0.12	0.12	0.11	0.00	0.01	0.06	0.14	0.01	0.02
Cr	0.00	0.00	0.00	0.00	0.00	0.00	0.01	0.00	0.00	0.00
Al	0.20	1.35	1.34	1.36	2.46	2.44	5.49	5.15	2.24	1.65
Fe^{3+}	0.50	0.12	0.13	0.12	0.28	0.28	-	-	0.15	0.51
Fe^{2+}	2.86	0.69	0.71	0.69	1.60	1.58	1.13	1.29	0.10	2.87
Mn	0.06	0.01	0.00	0.01	0.01	0.01	0.01	0.01	0.00	0.09
Mg	3.39	1.84	1.78	1.82	2.87	2.90	2.12	2.18	0.29	1.90
Ca	0.02	0.00	0.00	0.00	0.00	0.00	0.30	0.45	0.00	0.93
Na	0.02	0.03	0.02	0.02	0.00	0.00	0.52	0.46	0.05	0.30
K	0.00	0.84	0.87	0.85	0.00	0.00	0.03	0.00	0.84	0.05
OH	2.00	2.00	2.00	2.00	8.00	8.00	-	-	2.00	2.00

	anth 2536 c4	garn 2536 c4core	garn 2536 c4rim	garn 2536 in tm	chlor 2536 c4#1	chlor 2536 c4#2	tourm 2536 c1core	tourm 2536 c1rim	tourm 2536 blue	tourm 2536 green
SiO_2	50.68	36.31	36.50	36.35	24.59	54.79	35.65	35.12	35.38	35.87
TiO_2	0.02	0.17	0.11	0.08	0.10	0.03	0.13	0.32	0.16	0.25
Cr_2O_3	0.02	0.02	0.00	0.00	0.00	0.00	0.06	0.05	0.00	0.02
Al_2O_3	1.33	20.32	20.58	20.49	19.95	19.96	31.31	30.04	28.17	32.56
Fe_2O_3	5.02	0.40	0.15	0.11	4.51	4.57	-	-	-	-
FeO	25.59	33.64	33.79	31.53	23.00	23.28	8.99	9.91	11.87	7.57
MnO	0.78	3.29	2.46	5.42	0.18	0.19	0.02	0.00	0.05	0.00
MgO	11.84	1.84	2.25	1.26	13.31	13.30	6.42	6.73	6.64	6.75
CaO	0.78	2.51	2.67	3.23	0.00	0.01	1.20	1.73	2.36	1.21
Na_2O	0.16	0.02	0.00	0.00	0.06	0.00	1.92	1.69	1.44	1.72
K_2O	0.00	0.00	0.01	0.00	0.00	0.01	0.00	0.00	0.01	0.00
H_2O	1.96	-	-	-	11.05	11.10	-	-	-	-
Total	98.18	98.53	98.52	98.48	96.76	97.24	85.79	85.75	86.24	85.96
Si	7.76	2.99	2.99	3.00	2.67	2.68	5.81	5.78	5.87	5.78
Ti	0.00	0.01	0.01	0.00	0.01	0.00	0.02	0.04	0.02	0.03
Cr	0.00	0.00	0.00	0.00	0.00	0.00	0.01	0.01	0.00	0.00
Al	0.24	1.97	1.99	1.99	2.55	2.54	6.01	5.82	5.51	6.18
Fe^{3+}	0.58	0.03	0.01	0.01	0.37	0.37	-	-	-	-
Fe^{2+}	3.28	2.32	2.32	2.18	2.09	2.10	1.23	1.36	1.65	1.02
Mn	0.10	0.23	0.17	0.38	0.02	0.02	0.00	0.00	0.01	0.00
Mg	2.70	0.23	0.27	0.15	2.15	2.14	1.56	1.65	1.64	1.62
Ca	0.13	0.22	0.23	0.29	0.00	0.00	0.21	0.30	0.42	0.21
Na	0.05	0.00	0.00	0.00	0.00	0.00	0.61	0.54	0.46	0.54
K	0.00	0.00	0.00	0.00	0.01	0.00	0.00	0.00	0.00	0.00
OH	2.00	-	-	-	8.00	8.00	-	-	-	-